Investigation of the Spatio-Temporal Variations in Atmosphere Thickness Pattern of Iran and the Middle East with Special Focus on Precipitation in Iran

Iman Rousta [1],* , **Mehdi Doostkamian [2],*** , **Allah Morad Taherian [2]** , **Esmaeil Haghighi [3]** ,
Hamid Reza Ghafarian Malamiri [1] and **Haraldur Ólafsson [4]**

[1] Department of Geography, Yazd University, Yazd 8915818411, Iran; hrghafarian@yazd.ac.ir
[2] Department of Geography, University of Zanjan, Zanjan 3879145371, Iran; morad.taheriyan69@yahoo.com
[3] Department of Geography, University of Tabriz, Tabriz 5166616471, Iran; es_haghighi@ut.ac.ir
[4] Department of Physics, University of Iceland and Icelandic Meteorological Office, Bustadavegur 9,
    IS-150 Reykjavik, Iceland; haraldur@vedur.is
* Correspondence: irousta@yazd.ac.ir (I.R.); s.mehdi67@gmail.com (M.D.); Tel.: +98-9171902098 (I.R.)

Abstract: In this study, Geopotential Height (between 500 and 1000 hPa) and precipitation data were obtained from the NCEP/NCAR and IRIMO (Iran Meteorological Organization) for 60 years (1950–2010), respectively. Descriptive features of Atmospheric Thickness (hereafter AT) were calculated and analyzed by using the Mann-Kendall method. The results showed that the maximum AT was recorded in summer because of the dominance of the dynamic, hot subtropical high pressure. Furthermore, upper latitudes experienced more variations in terms of AT. The trend of variations showed that AT has significantly increased in recent years. Further, Saudi Arabia and the Red Sea experienced a more measurable increase in AT. On the other hand, AT had a declining trend over northern parts of Iraq and Iran, but it failed to be statistically considerable. The trend of AT had numerous variations over western parts of Iran, northwestern parts of Iraq, central and eastern parts of Turkey, and a large area of Syria. AT analysis of Iran's precipitations showed that patterns in the Sea Level Pressure were caused by East Mediterranean, Sudan, and Saudi Arabia low pressures and the high pressures that were located in Europe and Kazakhstan. In addition, in upper-air (500 Hpa), the patterns were influenced by high Mediterranean trough and blocking phenomenon that come from higher latitudes.

1. Introduction

Thickness maps are frequently used in synoptic climatology. These maps indicate the Atmospheric Thickness (AT) between the two layers of 500 and 1000 hPa, which is represented as the thickness of the entire atmosphere [1]. Atmospheric thickness, defined as the vertical distance between the 500- and 1000-mb pressure surfaces, is directly related to the mean temperature and water vapor path of an atmospheric layer [2]. A useful approximation to advection is obtained by regarding the thickness lines as material lines that are embedded in the surface geostrophic wind field [3]. Maps with the same thickness are indicative of places where cold or hot air is accumulated. Areas where contours are close together and have the lowest thickness are the regions in which cold air is accumulated. These regions represent low pressure areas on the earth and upper levels. On the contrary, areas where contours are close together and have the highest thickness demonstrate regions

in which hot air is accumulated. These areas represent high pressure regions on the earth and upper levels. Furthermore, the density of contours with similar thickness indicates areas where cold and hot weathers meet. These areas are known as discontinuity regions. A large proportion of atmospheric events takes place in these discontinuous and baroclinic zones. On the other hand, the continuation of iso thickness contours shows thermal wind, which indicates the overall condition of airflow in the layer. As a result, maps with similar thickness are useful tools for identifying air masses, fronts, and the path of atmospheric systems [4]. AT maps are among the most important upper-air and synoptic maps that are used in synoptic climatology to make predictions [5]. Such maps not only indicate the degree of coldness/hotness of air in the atmosphere, but also indicate the movement of cold and hot air masses. AT variations are caused by the advection of external air masses, dynamic ridge/trough of air, and heating/cooling on the earth's surface [6]. Studying contours with similar thickness can reveal areas where cold/hot air or tongue of cold/hot air is concentrated [7]. Iran is an area with anomalous and irregular precipitation [8–14]. Due to the variety of precipitation factors in different regions of Iran, the amount and time of precipitation from one place to another is significantly different [15–17]. Zhang et al. (1997) demonstrated that AT has a profound effect on the radiation of atmospheric downward longwave and snow melting. They showed that, in the thicknesses of 4850 m and 5450 m, there are radiations of 130 w/m^2 and 280 w/m^2, respectively [18]. In order to identify circulation patterns associated with Greece's extreme precipitation, Houssos et al. (2008) classified AT data on days with extreme precipitation. They identified nine circulation patterns of AT [19]. Some of the other research projects that concentrated on Iran's precipitation are as follows: Azizi et al. (2008) investigated severe cold waves of late December 2007 and early January 2008 in Iran by studying the structure of AT and air advection [20]; Soltani et al. (2014) and Asakereh (2012) investigated extreme precipitation in Kerman and Zanjan provinces [21,22] and Soltani et al. (2013) investigated the long-term precipitation in Gorgan province [23]; Sanders and Davis (1988) examined anomaly patterns of AT during cyclogenesis in the western part of central areas of the North Atlantic Ocean [24]; and, Struthwolf (1995) estimated the maximum temperature using an adjusted procedure of thickness layers between 700 and 850 hPa. He claimed that this procedure is highly efficient [25]. Iran's pervasive frosts occur alongside contours that have a thickness of 5300 to 5400 geopotential meters. In fact, pervasive frosts occur alongside these contours that are as thick as the atmosphere (especially the ones that are 5300 geopotential meters thick) [26]. In some other studies, AT patterns have been used to justify extreme precipitation. Some of these research projects include Mohammadi [27], Hosseini [28], Soltani et al. [29] and Halabian and Pourjazi [30].

Variations of upper-air thickness is related to anomalies in the surface climate. The study of thickness patterns as one of the tools for identifying and managing natural hazards, plays a significant role in preventing economic and human losses. Overall, few studies have focused on AT in Iran and across the world. There is not any published research studying the relation between AT and Iran's precipitation. Therefore, the present study sought to examine AT in Iran and the Middle East and its relation to Iran's precipitation.

2. Materials and Methods

2.1. Description of the Study Area Data Analyzed

The current paper aimed to investigate temporal and spatial variations in AT pattern of Iran and the Middle East, with a special focus on Precipitation in Iran during recent decades (1950–2010). The study area is located in longitudes and latitudes 25° to 68.5° E and 15° to 45° N (Figure 1).

To this end, geopotential height pressure data for 1000 and 500 hPa were obtained from NCEP/NCAR database for an area located between 25° to 68.5° E and 15° to 45° N. This group of data was used for extracting AT in study area. Then, in order to investigate the effect of atmosphere thickness on pervasive precipitation of Iran, daily precipitation data were collected from Iran Meteorological Organization (IRIMO). Environmental data that were used in this study came from two resources.

The first one included interpolated daily precipitation data for a period ranging from 1961 to 2004. These data had been prepared by Seyyed Abolfazl Masoodian in University of Isfahan, forming Asfazari database. The data of this database have a spatial resolution of 15 × 15 km, have been produced in the form of Lambert Conformal Conic Projection, and have been arranged in the form of a 7187 × 18,262 matrix with an S makeup (time in rows and place in columns) [31–33]. All of the data quality control of this database was conducted by Seyyed Abolfazl Massoodian in Isfahan University and it is approved by the Iranian Climatologists [34–37]. In order to completely collect data for the whole 50-years statistical period and have a more accurate database, the second group of data belonging to a time interval ranging from 1960 to 1961 and from 2005 to 2010 were collected based on precipitation data obtained from 553 synoptic and climatology stations of IRIMO. This second group of data was interpolated by using same method that is utilized in Asfazari database.
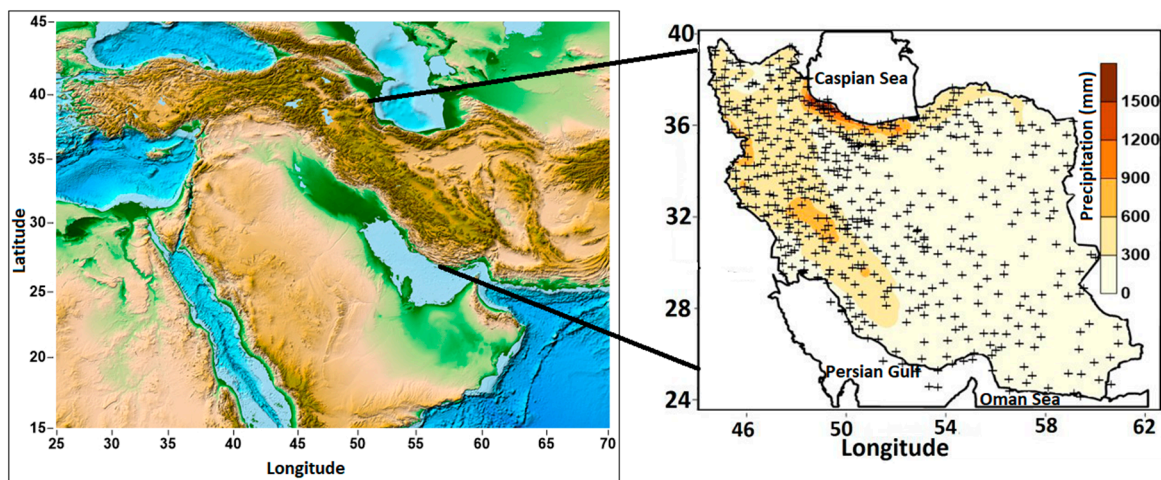
Figure 1. The study regions (Middle East) (A), Annual average precipitation (mm) distribution in Iran during 1951–2010 (shading), and the locations of all meteorological stations (+).

2.2. Statistical Methods

At first, to gain an overall picture of AT, descriptive features of AT were analyzed. Thickness maps, which show the layers between 500 and 1000 hPa, are frequently used in synoptic climatology. This thickness is regarded as the thickness of the entire atmosphere. AT increases as a result of hot weather and declines under the influence of cold weather. In fact, by studying the thickness between these two layers (500 and 1000 hPa), the thickness of the entire atmosphere is investigated. The following equation, which is known as hypsometric equation, is used to calculate AT:

$$tThickness = HGT_{500} - HGT_{1000} \tag{1}$$

If an object is expanded as a result of rise in temperature, its density will reduce. In contrast, if an object is shrunk by the rise of temperature, its density will go up. Therefore, with the fall of cold air, air mass becomes denser (thus, its density goes up), and, subsequently, the atmosphere becomes thicker. On the contrary, with the fall of hot air, air mass is expanded (hence, its density decreases) and molecules tend to diverge, which results in the increase of AT [26]. Thickness is one of the most important features of atmospheric dynamics and is under the influence of atmosphere temperature. The thickness of atmosphere can indicate cold or hot weather [38]. Furthermore, it can impact other atmospheric characteristics. As a result, thickness maps receive due attention in studying some

atmospheric events like frosts. In general, AT refers to the distance between the two layers of 500 and 1000 hPa [39]. More precisely, thickness is:

$$Z - Z_0 = \frac{RT}{g} \log \frac{p_0}{p} \tag{2}$$

where Z_0 and p_0 are, respectively, height and pressure in the reference level or the level just below the studied layer. If instead of fixed temperature we use average temperature all across the layer, then:

$$Z - Z_0 = \frac{RT_m}{g} \log \frac{p_0}{p} = \partial Z \tag{3}$$

In this equation, AT is calculated for the level between p_0 and p and in the T_m temperature.

After extracting AT, we used regression analysis for studying temporal and spatial variations in AT, and *t*-test for testing the statistical significance. The significance level in this study was 95% with an error value of 0.05.

After identifying AT, cluster analysis was used to assess thickness patterns of pervasive precipitations in Iran. In this study, a rainy day was defined as a day with a minimum precipitation of 1 mm. After identifying the rainy days, the coverage percentage (pervasiveness of precipitation) was investigated. The majority of researchers have used 50% coverage as the cut-off point for identifying pervasive precipitation. Therefore, the same criterion was used in this study. Cluster analysis was also used in the following step to classify data related to AT and identify representative days. In cluster analysis, variables are grouped in the light of particular features that are determined by the researcher. The purpose of conducting cluster analysis is finding real categories and reducing the bulk of data. In other words, cluster analysis is aimed at coming up with a smaller number of groups, so that similar data will be classified in the same category. This will minimize within group variance, while maximizing between group variance. In cluster analysis, grouping of data is carried out based on the distance or similarity among them. There are different procedures for measuring the distance among data. One of the most widely used procedures is the Euclidean distance method.

Lund correlation method was utilized to identify representative days for the obtained groups of AT. In this procedure, the representative day of each group is the one that has the highest similarity with other days of the same group. The correlation coefficient indicates the degree of similarity between the patterns of two different maps. In this procedure, a cut-off point should be determined for the correlation coefficient. In such cases, the value of the correlation coefficient typically ranges from 0.5 to 0.7 [40]. The cut-off point of 0.5 was defined for determining representative days in this study. More precisely, the representative day of each group was the one that had a correlation of at least 0.5, with the largest number of other days in the same group.

The Mann-Kendall method was used for investigating the trends in AT time series in the whole study area. If the time series is long enough to be considered as a combination of all the possible realizations, it is described as ergodic [41]. If there are different realizations of a system, it is possible to check the stationarity, but if there is only one realization it is impossible to distinguish between trend or non-stationarity and very-low frequencies in the data [42]. If we want to study the high-frequency component or create a power spectrum of data to reveal periodic components in our time series, it is necessary to remove the trend or very low frequency components from our data. There are many de-trending methods like, pre-whitening [43], polynomial fits [44], and spline [45] In another study, Vautard et al. (1992) used the nonparametric test of Mann-Kendall [46] for global trend identification. The Kendall method works as follows:

Let xi, i = 1, 2, . . . , n be a time series, then k_r is the number of times that xi1 < xi2 for all i1, i2 = 1, 2, . . . , n such that i1 < i2. A coefficient (τ) can be defined as:

$$\tau = \frac{4k_r}{n(n-1)} - 1 \tag{4}$$

which is distributed normally with zero mean and standard deviation (δ), i.e.,:

$$\delta = \sqrt{\frac{2(2n + 5)}{9n(n - 1)}} \tag{5}$$

The statistical significance test is carried out based on null hypothesis of no trend (i.e., stationarity) and the hypothesis will be rejected when the value of τ is outside the interval of (-1.96δ, $+1.96\delta$), with 95% confidence level.

3. Results

3.1. Analysis of the Seasonal Variability of Atmospheric Thickness

Table 1 contains spatial features of AT for each month for Iran and the Middle East. The map of average spatial distribution and coefficient of variations of AT in winter for Iran (JFM) and the Middle East shows that the average AT and the coefficient of variation in January are 5522.5 m and 2.6 m, respectively. The difference between mean, median, and mode indicates the relatively high homogeneity of various layers of AT in the Middle East. Furthermore, the lack of change in AT can be inferred because skewness is equal to zero in January.

**Table 1.** Spatial features of Atmospheric Thickness (AT) for each month in Iran (m).

	Winter			**Spring**		
	January	**February**	**March**	**April**	**May**	**June**
Mean	5522.5	5534.4	5579.8	5649.5	5715.6	5773.5
Median	5518.9	5536.5	5586.6	5668.1	5744.4	5802.4
Mode	5277.3	5281.0	5349.9	5436.4	5528.3	5598.8
Variance	20,876.7	22,317.3	19,156.6	12,900.3	9287.3	6085.6
STDV	144.5	149.4	138.4	113.6	96.4	78.0
CV (%)	2.6	2.7	2.5	2.0	1.7	1.4
Variation Range	480.7	489.2	442.9	378.1	304.8	279.7
Skewness	0.0	−0.1	−0.2	−0.3	−0.4	−0.6
Elongation	1.6	1.6	1.6	1.7	1.7	2.2
Max	5758.1	5770.2	5792.7	5814.5	5833.2	5878.5
Min	5277.3	5281.0	5349.9	5436.4	5528.3	5598.8
	Summer			**Fall**		
	July	**August**	**September**	**October**	**November**	**December**
Mean	5804.4	5797.6	5746.6	5677.1	5607.5	5554.2
Median	5816.9	5809.7	5773.7	5708.5	5624.9	5557.7
Mode	5639.4	5642.7	5579.2	5483.6	5390.4	5323.2
Variance	3832.5	3668.8	5625.2	8764.0	13,201.6	17,382.0
STDV	61.9	60.6	75.0	93.6	114.9	131.8
CV (%)	1.1	1.0	1.3	1.6	2.0	2.4
Variation Range	263.2	249.1	260.9	309.8	388.3	439.6
Skewness	−0.7	−0.7	−0.8	−0.6	−0.3	−0.1
Elongation	2.8	2.7	2.3	1.9	1.7	1.6
Max	5902.6	5891.8	5840.2	5793.4	5778.7	5762.7
Min	5639.01	5642.7	5579.2	5483.6	5390.4	5323.2

Coefficient of variations in January (Figure 2) shows that 20° latitude (which covers areas over Sudan, Saudi Arabia, the Red Sea, the Arabian Sea, and the Persian Gulf) has had the lowest coefficient of variations (0.2) since these areas are influenced by homogenous air masses in January. Air masses with different features do not usually find their ways into this region. On the other hand, in regions that are located in upper latitudes to the north, the coefficient of variations of AT has increased, reaching a peak of 0.8. These areas are affected by various air masses in January.

However, the average of coefficient of variations of AT in most areas of the Middle East is 1.57. It has encompassed lower latitudes compared to January. In March, iso thickness contours are orbital and the coefficient of variation of AT in upper latitudes has less variation as compared to that of lower latitudes. This can be attributed to the fact that, during March, upper latitudes are influenced by various air masses which originate from the arctic, Mediterranean, etc.

The average AT in the Middle East has increased in spring (AMJ) when compared to winter (5649.5 m in April and 5773.5 m in June). This rise in AT is due to the gradual withdrawal of cold air masses of upper altitudes and the gradually increasing influence of subtropical high pressure on the Middle East. The average AT has reached its peak in June. On the other hand, the highest value of coefficient of variations has been recorded in April rather than May (1.7) or June (1.4).

For the majority of areas in the Middle East, including Saudi Arabia, Iraq, Persian Gulf countries, and southeastern parts of Iran, the average of coefficient of variations of AT in April has been 0.36. The map of the spatial distribution of average of coefficient of variations of the AT for Iran and the Middle East in summer (JAS) (Table 1) shows that AT in the Middle East has had the highest mean in July (5804.4 m).
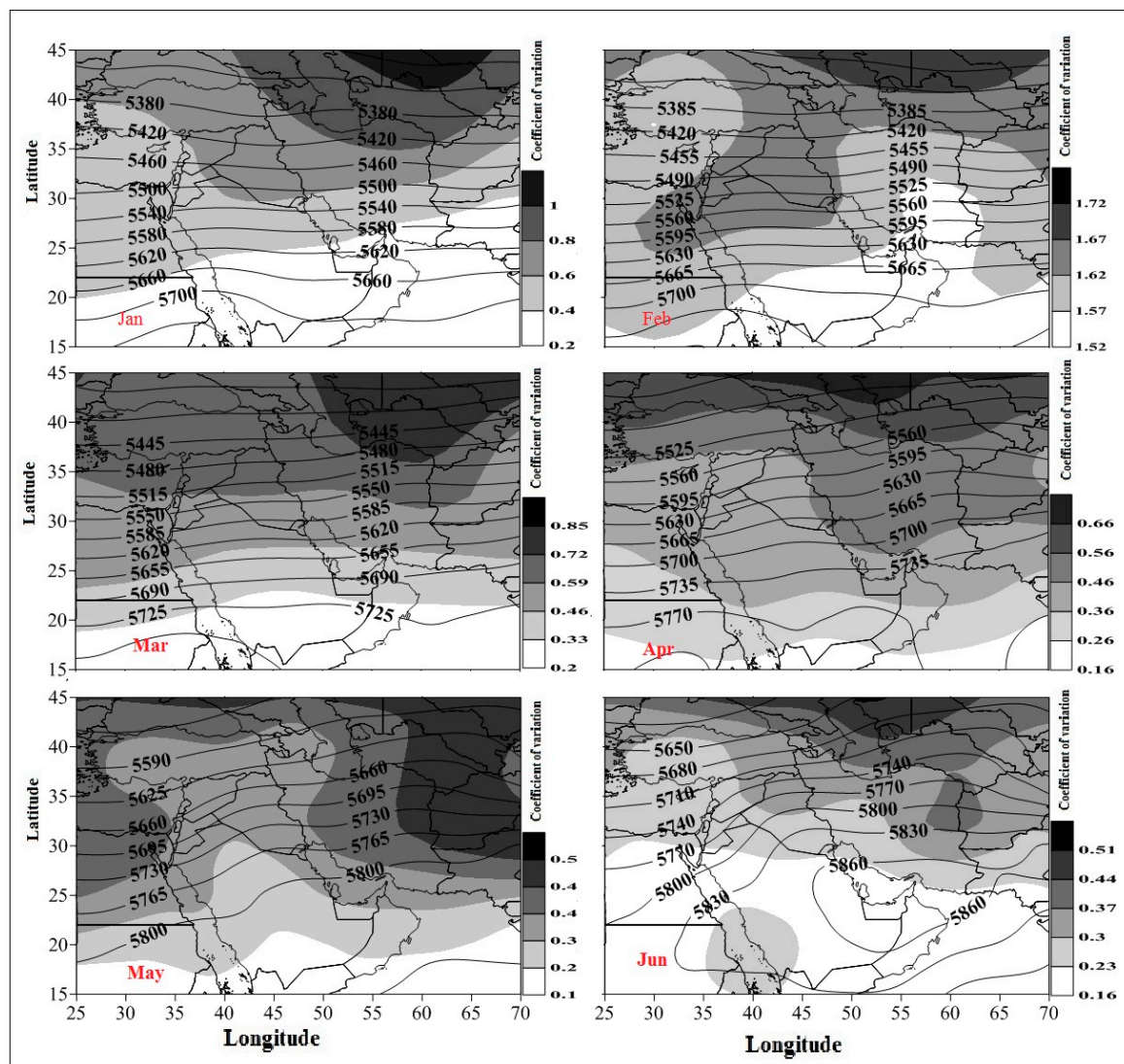
(A)

Figure 2. *Cont.*
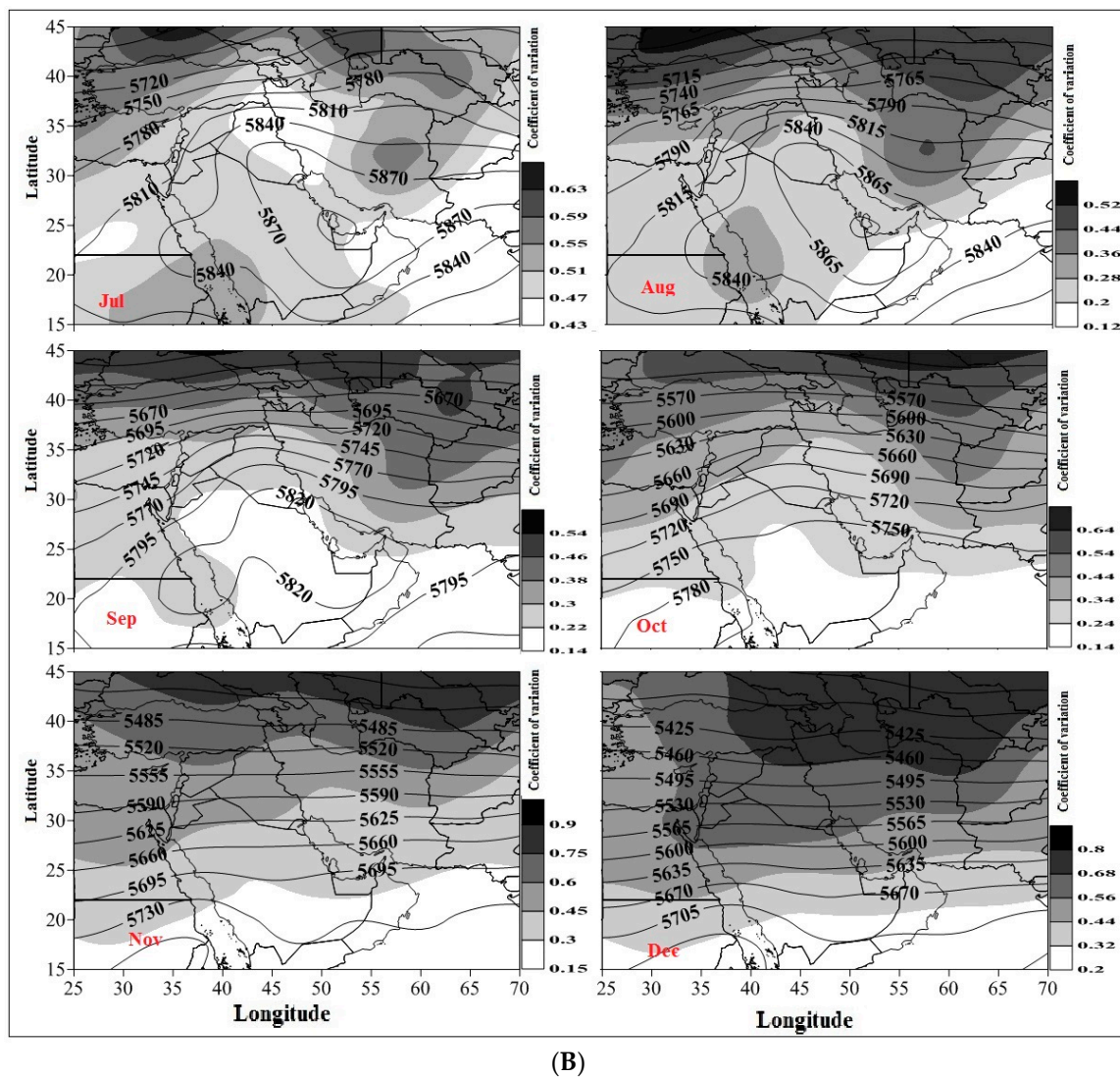
Figure 2. (**A**) Spatial distribution of average of coefficient of variation of AT in each month in Iran and the Middle East; (**B**) Spatial distribution of average of coefficient of variation of AT in each month in Iran and the Middle East.

Iso thickness contours of July, August, and September (Figure 2) indicate that the maximum density of thickness layers belongs to northeastern Iran, Iraq, Turkey, and Syria, while the minimum density has been registered for southern Saudi Arabia, southern Iran, and some parts of the Red Sea, areas that have a high temperature during summer. Temperature declines toward upper latitudes, hence higher density and lower thickness of atmosphere. In summer, the lowest coefficient of variations of AT in the Middle East (0.12) was recorded in August and belonged to southern Saudi Arabia, the Arabian Sea, and southern parts of the Persian Gulf. The second lowest coefficient of variations of AT in the Middle East (0.14) was recorded in September, and it belonged to Saudi Arabia, southern Iraq, areas around the Persian Gulf, and the Arabian Sea. There is a small difference among indices of central tendency (mean, median, and mode) of the AT in the Middle East during summer. Thus, there has been more homogeneity among various layers of AT during this season. The highest AT for the entire year has been recorded in July (5804.4 m). This indicates that July has the highest temperature, hence this month has experienced the maximum expansion in atmosphere layers.

The spatial distribution map of average of coefficient of variations of AT in Iran and the Middle East during fall (Table 1) shows that the average AT in the Middle East has had the highest coefficient of variations in this season (5677.1 m in October, 5067.5 m in November, and 5554.2 m in December).

3.2. Analysis of the Interannual Variability of Atmospheric Thickness

Spatial–temporal variation of AT during winter in the Middle East (Figure 3) shows that a negative thickness trend has been experienced in January and February, while there has been no negative trend in March. In January, there has been a positive AT trend to the latitude of 25° covering areas that include Saudi Arabia, Persian Gulf countries, and southern Iran. On the contrary, Iraq, Turkey, and northern parts of Iran have had a negative trend. The positive AT trend in January has ranged from 11 m in Saudi Arabia to 15 m in the Arabian Sea. By contrast, the sharpest negative trend of AT belongs to northern areas (−18 m) and eastern Iraq (−10 m) in February. In January, two regions have had totally different thickness trends in the Middle East; the first area involves western and southwestern parts of Iran and central and eastern parts of Turkey, which have experienced a negative trend. On the other hand, areas over the Black Sea have had a positive trend. Thus, there has been a huge trend difference between these two regions. The type and percentage of AT trend in Iran and the Middle East during January shows that, in total, 27.1% of the study region has been a rising significant trend and the rest of area (72.3%) has not been any significant trend. In February, the negative AT trend has dominated the largest parts of the Middle East. In addition, the positive trend of this month has been weaker than that of January. In the Middle East, the largest area with a positive trend of AT belongs to southern Saudi Arabia and the Arabian Sea (6 to 8 m). Except for these areas, latitudes upper than 25° have had a negative trend. The maximum negative trend of AT (−10 to −18 m) belongs to Turkey, as well as northwestern and northern Iran. In February, the maximum difference in the trend of AT has been registered for western parts of Iran. 100% of study area has not been any significant trend. In winter, the widest positive trend of AT in Iran and the Middle East has been recorded in March. In this month, overall, 27.9% of the study area has been rising significant trend, whereas 71.1% has not experienced any significant trend.

Table 2 showed the AT monthly trend of the atmosphere of Iran based on Mann-Kendall method. As seen in this table, the AT has been increasing for all of the months in the whole statistical period. This trend has been significant for all of the months except January, February, and December. The highest trend of AT occurred in the August ($0/346$ (m/m)).

Spatial–temporal variations of AT I n the Middle East in spring (Table 3) shows that, in April and May, all of the Middle East (except for eastern Turkey) has had a positive trend. The sharpest positive trend of AT has been registered for southern Saudi Arabia and the Persian Gulf in April (18 m) and May (19 m). The difference in the trend of AT, which dominates eastern Turkey in April, can also be observed in May. The entire Middle East has had a positive AT trend in June. No negative AT trend can be observed in the entire region in this time. The type and percentage of the AT trend of Iran and the Middle East in April shows that 44.9% of the Middle East has been a rising significant trend and 55.1% of the area has not been any significant trend. In May, the areas with the highest positive thickness trend (13 to 19 m) are located in southern Saudi Arabia, eastern Iraq, southern Iran, the Persian Gulf, and some areas of the Arabian Sea. In this month, only eastern Turkey has had a negative AT trend (−1 to −5 m). The type and percentage of AT in Iran and the Middle East in May shows that, in total, 60.7% of study region has been a rising significant trend, whereas 39.3% of Middle East has not been significant trend. In June, the percentage of areas covered by the AT trend in Iran and the Middle East shows that, overall, 80.2% of Middle East has experienced a rising and significant trend and 19.8% of the region has not been any significant trend.

Table 2. AT monthly trend according to Mann-Kendall method during 1950–2010 (60 years) (meter per month (m/m)).

Month	January	February	March	April	May	June
Trend	0.126	0.075	0.287	0.301	0.319	0.345
Significance	1	1	0	0	0	0
Month	**July**	**August**	**September**	**October**	**November**	**December**
Trend	0.284	0.346	0.295	0.320	0.308	0.247
Significance	0	0	0	0	0	1

3.3. Analysis of the Link between Atmospheric Thickness and Precipitation in Iran

In order to study the effect of AT on pervasive precipitations in Iran, after identifying Iran's precipitation days, the thickness data for these days were extracted. Then, cluster analysis was performed on the thickness data. Cluster analysis is the art of finding groups in data. The classification of similar objects into groups is an important human activity. Cluster analysis can be used not only to identify a structure that is already present in the data, but also to impose a structure on a more or less homogeneous data set that has to be split up in a "fair" way [47,48]. Finally, by using trial and error and variance analysis, four thickness patterns for Iran's pervasive precipitation were selected (Figure 4).

Table 3. Area (%) covered by AT in Iran and the Middle East (In this table: Decr = Decreasing, Incr = Increasing).

| Month	Type of Trend	Coverage (%)	Month	Type of Trend	Coverage (%)
January	Decr	0	July	Decr	0
	Incr	27.2		Incr	88.8
	No Trend	72.8		No Trend	11.2
Februsry	Decr	0	August	Decr	0
	Incr	0		Incr	62.8
	No Trend	100		No Trend	37.2
March	Decr	0	September	Decr	0
	Incr	27.9		Incr	61.1
	No Trend	72.1		No Trend	38.9
April	Decr	0	October	Decr	4.9
	Incr	44.9		Incr	61.5
	No Trend	55.1		No Trend	38.5
May	Decr	0	November	Decr	0
	Incr	60.7		Incr	47.8
	No Trend	39.3		No Trend	52.2
June	Decr	0	December	Decr	0
	Incr	80.2		Incr	34.8
	No Trend	19.8		No Trend	65.2

Figure 5 displays the spatial distribution of synoptic-dynamic patterns of the representative day for the first pattern (belt of Mediterranean-Caspian Sea low pressure and North European high pressure). The sea level pressure map (Figure 5) shows that a wide low pressure belt has dominated the northern parts of the Middle East, ranging from eastern Mediterranean to northern Iran. It constitutes a closed curve, with its central core having a pressure of 1004 hPa dominating east Mediterranean through the Caspian Sea. It is combined with the low pressure system of southeastern Russia and eastern Ukraine. Also, the European high pressure, which has a central pressure of 1038 hPa, has dominated northern Europe.

In order to have a better analysis of atmosphere condition and identify precipitation productive systems in Iran, iso height contours of 500 hPa and AT have been illustrated in Figure 5. Iso height contours of 500 hPa show that a low pressure center with a contour of 5180 geopotential meter has been shaped over Eastern Europe and central parts of Ukraine. This low center, which can be called an atmospheric coldhole, completely affects AT because of its high atmosphere density. Thus, the lowest AT (5120 m) is completely in line with the atmospheric coldhole of 500 hPa.


(A)

Figure 3. *Cont.*

(**B**)
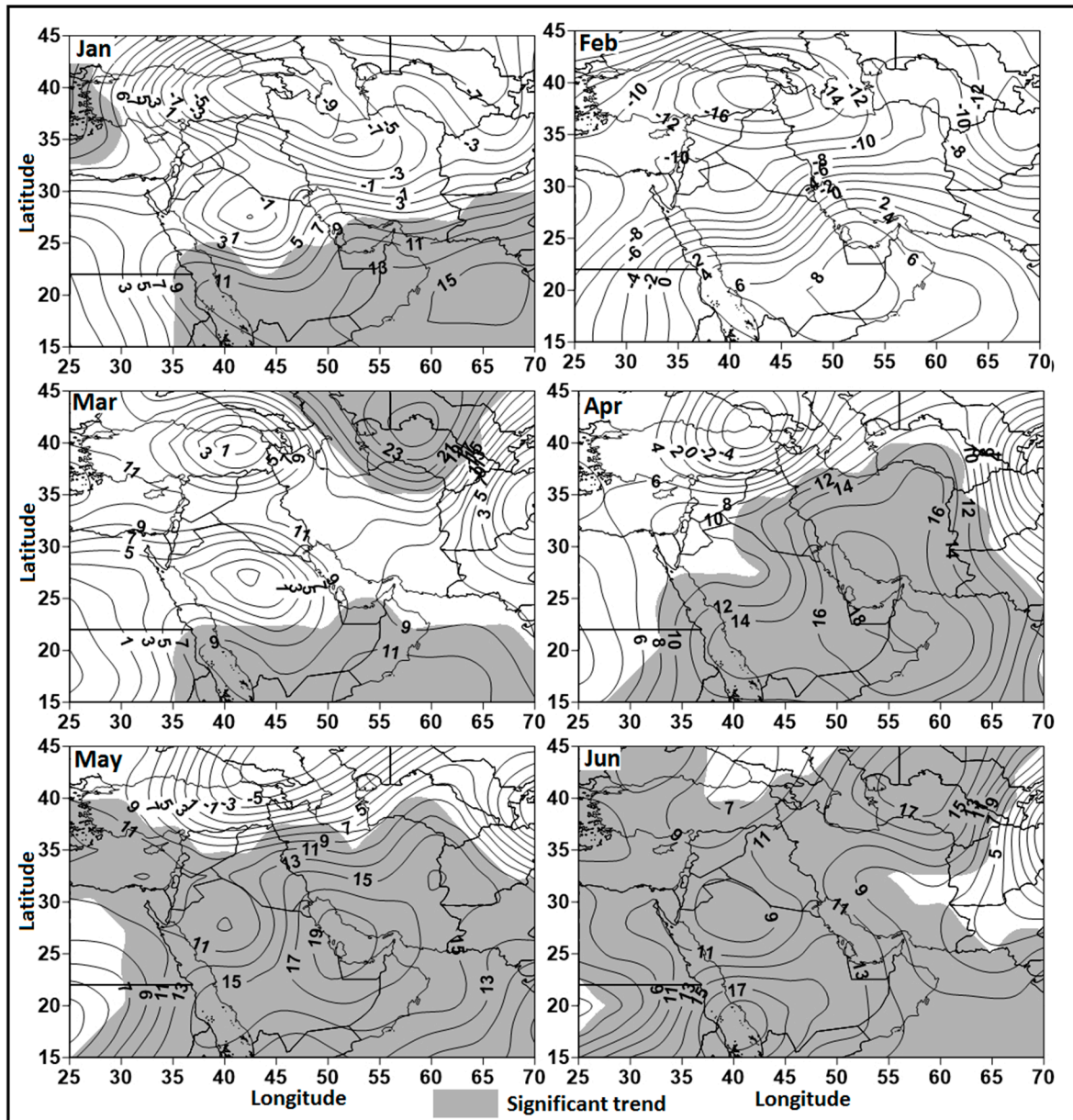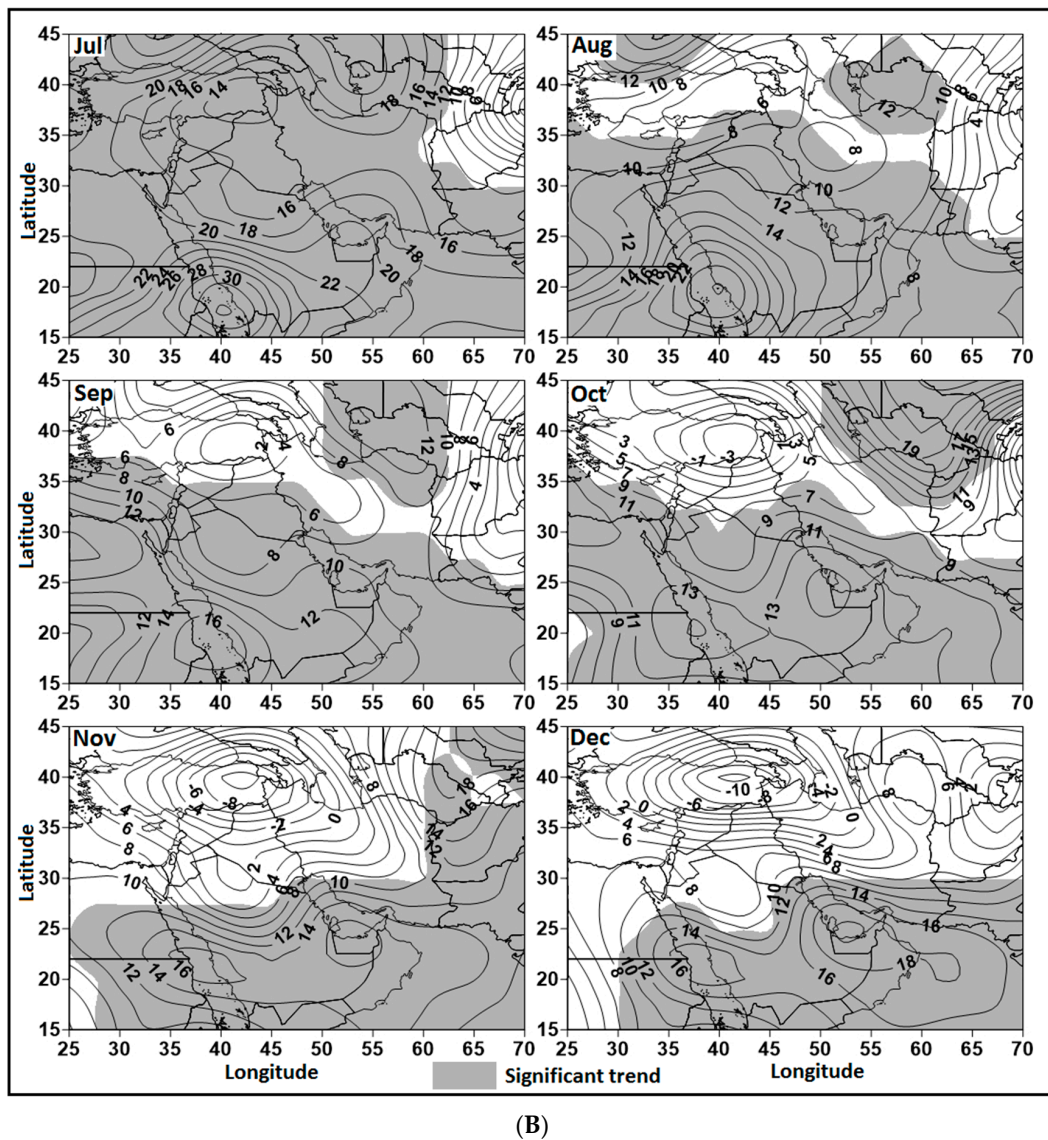
Figure 3. (**A**) Spatial distribution of Iran's monthly trend, AT and level of significant; (**B**) Spatial distribution of Iran's monthly trend, AT and level of significant.

Figure 5 displays the spatial distribution of synoptic-dynamic patterns for the representative day for the second pattern (Kazakhstan high pressure, Mediterranean low pressure, and Sudan). The sea level pressure map (Figure 5) shows that a low pressure system dominates the eastern Mediterranean with a central pressure of 1009 hPa. It is moving in a cyclonic manner toward northern regions of the Middle East. At the same time, in northern parts of Africa, Sudanese low pressure is moving toward upper latitudes with a central pressure of 1017 hPa.

Figure 5 displays the spatial distribution of synoptic-dynamic patterns for the representative day for the third pattern (Saudi Arabia high pressure and Turkmenistan low pressure). The sea level pressure map (Figure 5) shows that a high pressure system, with a central pressure of 1018 hPa, has been formed over Saudi Arabia and has stretched to the latitude of 35° north and the longitude of 60° east.
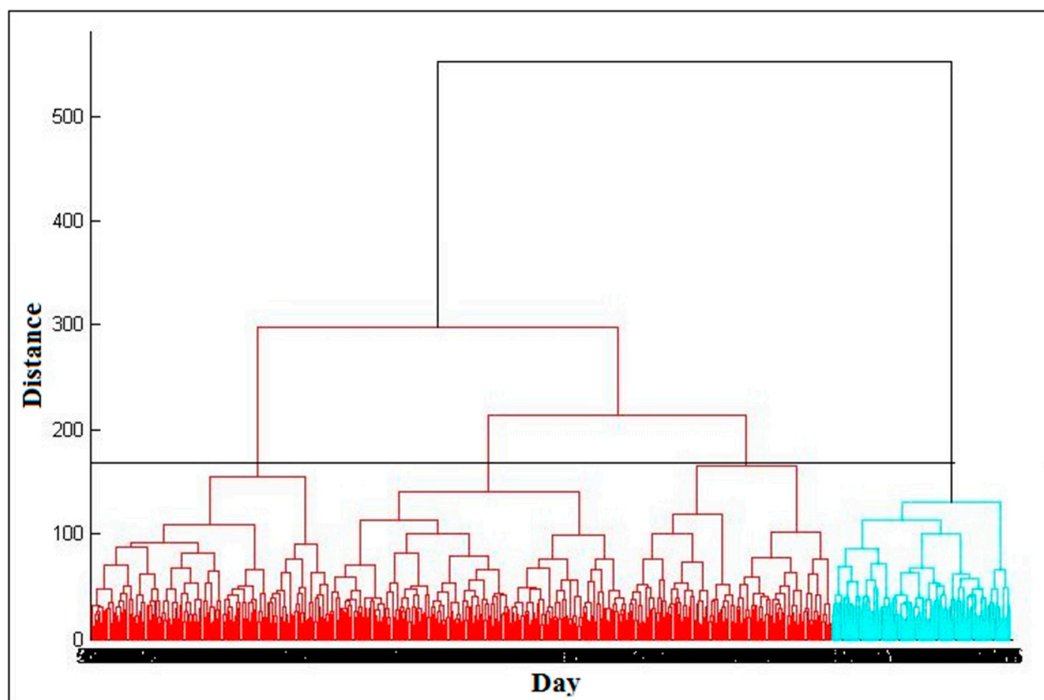
Figure 4. The dendrogram obtained as a result of conducting cluster analysis for AT during pervasive precipitation in Iran.

Figure 5 displays the spatial distribution of synoptic-dynamic patterns for the representative day of the fourth pattern (the belt of Mediterranean low pressure, the Black Sea–Saudi Arabia low pressure). The sea level pressure map (Figure 5) shows that a strong cyclonic system has been formed over eastern regions of the Mediterranean, and has been combined with the Black Sea and Kazakhstan low pressure, shaping a wide low pressure belt over northern parts of the Middle East.

In order to investigate the seasonal analysis of the effect of AT on Iran's precipitation, the effect of AT in fall on the precipitation of Iran was studied and analyzed because this season has high variability coefficient as compared with other seasons of Iran.

The spatial-temporal distribution of the precipitation pattern of fall for the AT in the Middle East (Figure 6A) shows that a deep trough has stretched over the western regions of the Mediterranean and northern Africa and Algeria. Although this trough is deep, its wavelength is not wide and it does not influence a large area. Since the western part of the trough has negative vorticity, it results in the advection of cold and humid air from the Mediterranean toward northern regions in the Middle East. However, in central parts of the Middle East, it has formed mass or ridge, causing the advection of hot air.

The spatial-temporal distribution of the second precipitation pattern of fall for the AT in the Middle East (Figure 6B) shows that a low height system, with a central pressure of 5380 geopotential meter, has been formed in northern Europe and has crossed the Black Sea to reach the Middle East.
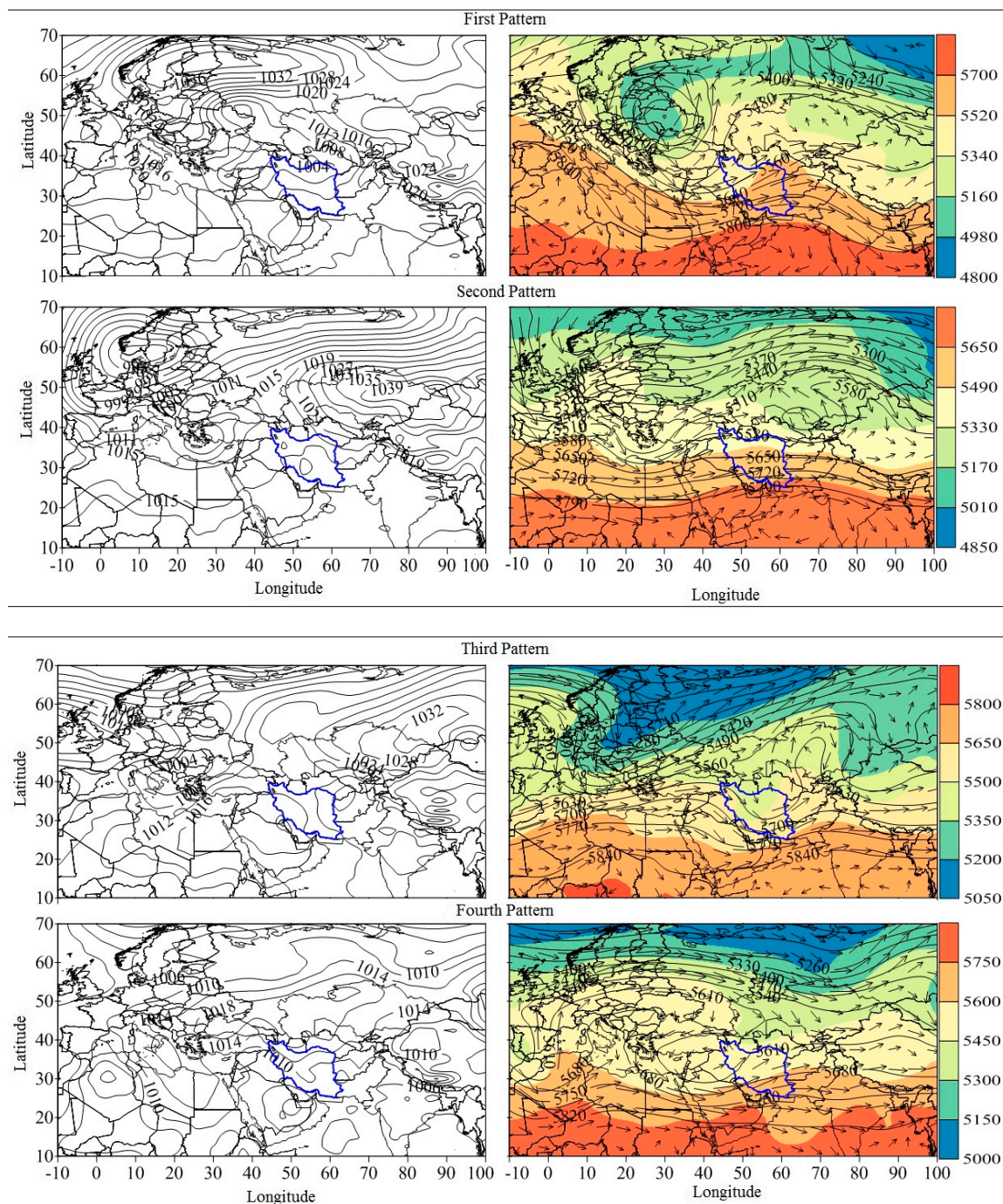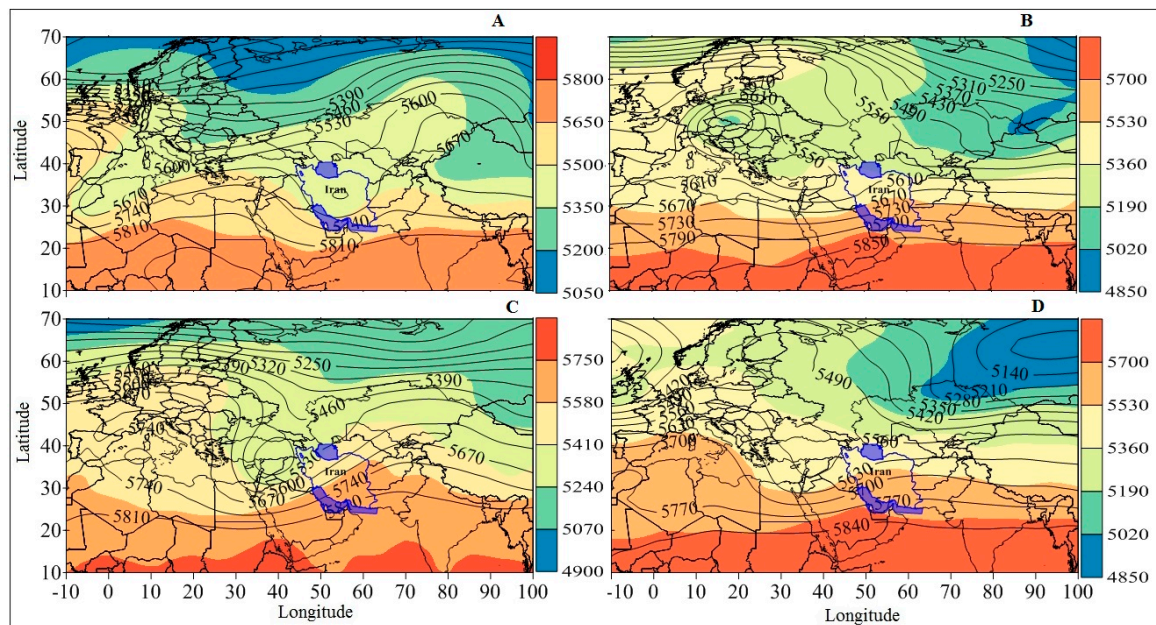
Figure 5. The thickness patterns of the Iran's comprehensive precipitation.

The spatial-temporal distribution of the third precipitation pattern of fall for the AT in the Middle East (Figure 6C) shows that two low height cores have dominated the Mediterranean and southwestern Europe.

The spatial-temporal distribution of the fourth precipitation pattern of fall for the AT in the Middle East (Figure 6D) shows that the formation of a ridge over Europe and the location of its eastern part over Eastern Europe have directed cold air toward the lower latitudes and northern parts of the Middle East. Thus, AT has declined to its lowest degree (5350 m) in northern regions of the Middle East. At the same time, a low system with a cold core with a cyclonic movement has been formed over North Africa.

Figure 6. The thickness patterns of the Iran's fall comprehensive precipitation; (**A**) a deep trough on the western Mediterranean; (**B**) low height system on the Europe; (**C**) two low height cores on the Mediterranean and southwestern Europe; (**D**) a ridge over the Eastern Europe.

4. Discussion

4.1. Seasonal Variability of Atmospheric Thickness

The density of air flow contours in Figure 2 demonstrates that a highly thick layer over Saudi Arabia, the Red Sea, and the Arabian Sea has led to the maximum AT (5560 to 5720 m) over southwestern areas of the Middle East. For the same reason, the average coefficient of variations for southern parts of the Red Sea, southern Saudi Arabia, the Arabian Sea, and south and southeast of Iran is 1.57, in January. The seasonal variability of atmospheric thickness shows that the highest and lowest AT belong to March and January, respectively (Table 1). This shows that, in the Middle East, the average temperature in March has been higher than that in February and January, a phenomenon that has led to the expansion of upper atmosphere layers in March. In January, however, the low average temperature has resulted in the shrinkage of atmosphere layers. This condition might be due to the fact that, in winter, the Middle East is influenced by various pressure systems (Red Sea low pressure, North African high pressure, Northeastern Iran high pressure, European high pressure, and North Caspian Sea high pressure), causing changes in its climate [49]. Since most of these masses contain cold air, they considerably reduce the AT.

The average AT peak was seen in June and the highest value of coefficient of variations has been recorded in April rather than May (1.7) or June (1.4). This is due to the fact that, in April, the Middle East is still under the impact of cold wind waves of upper latitudes. The difference between the mean, median, and mode of AT in the Middle East is greater in spring than winter. Therefore, homogeneity in spring is lower than that in winter. The variability of AT can be clearly inferred from the values of negative skewness (April, May, and June).

The highest mean of AT in the Middle East in July (5804.4 m, Table 1) indicates that, in summer, the middle and upper level of atmosphere in the Middle East is influenced by Azores high pressure (which is the only high pressure center during the hot season of the year). Azores high pressure functions differently in Asia and Africa during the hot season of the year. However, geographical features of Azores high pressure centers in Asia and Africa are regarded as the main factors that control the climate of the Middle East during the hot season of the year (Zarrin et al., 2010). On the other

hand, a high temperature of atmosphere in the Middle East during summer is attributed to sun's perpendicular radiation, air expansion, and high AT [50]. Therefore, the lowest coefficient of variations of AT has been recorded in summer because, in this season, the Middle East is typically influenced by homogeneous air masses of Azores high pressure. The nature of these air masses is more similar in summer when compared to the air masses of other seasons.

Various pressure systems affect the temperature of the Middle East during cold seasons (fall (OND) and winter) and, consequently, influence AT. For example, the Red Sea low pressure dominates some parts of the Indian peninsula, the Indian Ocean, African lands (except for Algeria, Tunisia, Libya, Egypt, and Ethiopia), and the Red Sea. Furthermore, Oman low pressure influences a region ranging from Ethiopia to the Arabian Sea and the Indian peninsula. It also dominates northern Pakistan to the west of the Mediterranean. Moreover, European high pressure, Kazakhstan high pressure, northern Caspian Sea high pressure, Mediterranean low pressure, and Siberian high pressure have profound influence on the climate of the Middle East in that order [26,27,51,52].

The average AT in the Middle East has had the highest coefficient of variations in fall season (5677.1 m, Table 1). This can be attributed to the fact that fall is a transition period in the year. On the one hand, subtropical high pressure systems that dominate the area during hot seasons have not left the region yet. On the other hand, western winds and pressure systems that influence the area in cold seasons are moving toward the region. The highest coefficient of variations for the entire year belongs to December, fall (2.4%). The higher density of iso thickness layers in December (as compared to November and October) shows that temperature has been lower and layers have shrunk more and have had higher density in this month. Like other months of the year, southern Saudi Arabia, southern areas of the Arabian Sea, and southern regions of the Red Sea have had the lowest coefficient of variations in fall. In contrast, northern parts of Turkey, Syria, northern regions of Iraq, and northern Iran have had the highest coefficient of variations in this season.

4.2. Interannual Variability of Atmospheric Thickness

The spatial–temporal variations of AT in summer (July, August, and September) in Iran and the Middle East (Figure 3, Table 3) demonstrates that the whole region has had a positive trend of AT. The sharpest positive trend belongs to southeastern Saudi Arabia and the Red Sea (22 to 30 m in July, 16 to 22 m in August, and 12 to 16 m in September). The type and percentage of areas that are covered by the AT trend in the Middle East indicate that, in July and August, the Middle East has experienced a rising significant trend, respectively, with 88.3% of the study area in July and 62.8% in August. In September, 61.1% of Middle East has been a rising significant trend, and 38.9% of the region has not been any significant trend. The spatial–temporal variations of AT in fall (October, November, and December) in Iran and the Middle East (Table 3) indicates that the entire region (save for northern and northwestern Iran) has had a positive trend of AT. The sharpest positive trend belongs to southern Saudi Arabia, the Red Sea, and the Strait of Hormoz (13 to 15 m in October, 12 to 15 m in November, and 14 to 18 m in December). The steepest positive trend of AT has been registered in December over the Strait of Hormoz and the Gulf of Oman. The type and percentage of areas that are covered by the AT trend in the Middle East indicate that, in October, in total, 61.5% of the study area has experienced a rising significant trend, while 38.5% of the region has not been a significant trend. In November, 47.8% of Middle East has been rising significant trend. In December, 34.8% of Middle East has experienced a rising significant trend and 65.2% of the region has not been any significant trend.

4.3. The Relationship between the Atmospheric Thickness and Precipitation in Iran

4.3.1. Atmospheric Conditions Not Linked with Precipitation

A wide low pressure belt of the northern parts of the Middle East ranging from eastern Mediterranean to northern Iran (First Pattern) has been seen in Figure 5. The anti-cyclonic movement of the high pressure system and the suction caused by the low pressure system of northern parts

of Iran have moved the high pressure system toward lower latitudes. The dominance of severe ingredient pressure has led to air instability and vertical ridge. The dominance of high pressure over the Middle East and Iran, which is due to the presence of high pressure systems in western China, as well as northern and western Europe, has led to an unstable weather all over the Middle East. This is due to the fact that low pressure systems of northern regions of the Middle East have been surrounded by high pressure systems of neighboring areas.

The precipitation productive system in Iran was identified by the iso height contours of 500 hPa and AT (Figure 5). The low pressure center with a contour of 5180 geopotential meter is called Coldhole. Atmospheric coldhole is an obstacle that forces western winds to move toward lower latitudes, forming a deep trough over central and northern parts of the Middle East. The highest divergence of this trough is located over Iran and the lower pressure system on the surface of earth is positioned in northern regions of Iran.

The spatial distribution of synoptic-dynamic patterns for the representative day for the second pattern (Kazakhstan high pressure, Mediterranean low pressure, and Sudan) was shown in Figure 5. The low pressure system from eastern Mediterranean with a central pressure of 1009 hPa that is moving in a cyclonic manner is presented in Figure 5. The cyclones formed by this low pressure system have moved toward the latitude of 30° and have been located in the path of western winds. They have turned into dynamic entities and moved toward northern regions.

4.3.2. Atmospheric Conditions Linked with Precipitation

On the other hand, whenever Sudanese and Mediterranean low pressure come into contact, a trough is formed in eastern Mediterranean. If this trough is deep, it will cause heavy precipitation in most parts of Iran [53]. Strengthening the activities of Sudanese low pressure centers turns them into dynamic and thermodynamic systems, causing heavy precipitation in some areas of Iran, especially southwestern Iran. This Sudanese system usually enters Iran from several paths.

The main entrance of this system into Iran is when it is combined with Mediterranean low pressure, causing heavy precipitations [54]. This low pressure system moves over southern parts of the Middle East (the Red Sea and southern Saudi Arabia) entering the territory of the Persian Gulf and transferring humidity to southern and southeastern Iran. At the same time, Kazakhstan high pressure, which has a pressure of 1041 hPa, has been formed on the border with Mongolia. It has had an anti-cyclonic and westward movement reaching eastern and northeastern parts of Iran.

A low pressure system has entered Iran from the southeastern part. Therefore, the highest pressure and instability is located in two areas of Iran; the northwestern part, which is influenced by the Mediterranean and Sudanese low pressure, and the southeastern part. In order to have a better analysis of atmosphere condition and identify precipitation productive systems in Iran, iso height contours of 500 hPa and AT have been illustrated in Figure 5. It is demonstrated that the western flows are moving in large quantities in the form of zonal belts toward eastern regions of the Middle East.

However, in the eastern Mediterranean, a weak trough has been formed. In such a situation, the cold air of Europe can dominate the Mediterranean, confronting hot and humid weather of this area in cold weathers and preparing conditions for forming a front. On the other hand, the dominance of the trough over the Mediterranean provides an unstable dynamic condition. This condition, along with discontinuity-based instability, can provide the ground for the formation of rain systems [55].

The spatial distribution of synoptic-dynamic patterns for the representative day for the third pattern (Saudi Arabia high pressure and Turkmenistan low pressure) was shown in Figure 5. The high pressure system from eastern Mediterranean with a central pressure of 1018 hPa formed over Saudi Arabia and stretched to the latitude of 35° north and the longitude of 60° east, is presented in Figure 5.

Due to the presence of a low pressure system over southern parts of Europe, this high pressure system has moved toward east, with an anti-cyclonic movement. It has crossed the Red Sea, the Saudi Arabia peninsula, and the Persian Gulf, stretching over western, southwestern, and northwestern regions of Iran. Thus, the curve with a pressure of 1018 hPa is located over northwestern parts of Iran.

At the same time, Turkmenistan low pressure has been formed in central areas of Turkmenistan and Afghanistan. It has moved westward, it has entered Iran from the eastern part, and it has stretched to central regions of Iran. In central and southern parts of Iran, extreme pressure gradient has been caused by the presence of contours from Saudi Arabia high pressure, leading to weather instability and air ridge.

On the other hand, hot and humid masses have moved from the Indian peninsula and the Bay of Bengal toward southeastern and eastern regions of Iran. They have been combined with Turkmenistan low pressure. At the same time, in the atmosphere level of 500 hPa, Mediterranean trough with an iso height curve of 5600 geopotential meter has been located over central and southern Iran. Its positive vorticity and upper divergence is exactly in line with the maximum difference of sea level pressure.

On the contrary, western parts of Iran, which are located in the west of the trough and have experienced the cold air of upper latitudes, have the minimum AT (5290 m). The same condition exists for northern regions of the Middle East which are influenced by the cold air of Europe. However, southern parts of the Middle East, which are influenced by flows in northern Africa and the hot air of lower latitudes, have a thicker atmosphere compared to northern regions.

The spatial distribution of synoptic-dynamic patterns for the representative day for the fourth pattern (the belt of Mediterranean low pressure, the Black Sea–Saudi Arabia low pressure) was illustrated in Figure 5. The strong cyclonic system formed over eastern regions of the Mediterranean and was combined with the Black Sea and Kazakhstan low pressure, shapes a wide low pressure belt over northern parts of the Middle East (Figure 5).

The Mediterranean low pressure has moved toward lower latitudes reaching the north of Africa and Egypt. It has also moved eastward, crossing Mount Ararat in Turkey and entering Iran from northwestern and western areas. The cyclonic and meridional movement of Kazakhstan and the Caspian Sea low pressure has influenced northern and northeastern parts of Iran.

The Saudi low pressure enters Iran from western and southwestern parts after passing over the Persian Gulf. Also, the southeastern regions of Iran are influenced by the low pressure of the Indian Ocean and the Bay of Bengal. Thus, all the regions of Iran are under the influence of various low pressure systems, with each system transferring humidity to central Iran in one way or another.

At the same time, an omega shaped blocking system has been formed in the atmosphere level of 500 hPa (Figure 5) in southern Europe and northern regions of the Mediterranean. It has a central contour of 5680 geopotential meter. There is a huge high pressure at the center of this system, with its mass being stretched toward the north.

Cyclonic movements can be observed in its southwestern and southeastern parts. The cyclonic movement in its southwestern part is located over Iraq, Syria, and western regions of Iran. It has a wide trough. Also, cold air moves from Europe and the Mediterranean toward Iran. These factors along with the injection of humidity from the Persian Gulf, the Mediterranean, the Caspian Sea, and the Indian Ocean cause pervasive precipitations in Iran.

The effect of AT on Iran's precipitation in fall, as the season having highest variability coefficient when compared with other seasons of Iran, was studied and analyzed (Figure 6A). AT is influenced by the type of air dominating a region. Thus, the highest AT has been recorded in southern areas of the Middle East including southern Saudi Arabia, the Arabian Sea, and the Persian Gulf. This is due to the fact that, in fall, the atmospheric systems of upper latitudes are not strong enough to move toward lower latitudes of the region. The lowest AT is located in central Iran, which is in line with the low dynamic system.

On the other hand, a low system with a cold core is located over central parts of Iran. The minimum AT in the Middle East is in line with this low system. Its falling arm has moved cold air toward lower latitudes, influencing Iraq, Saudi Arabia, southwestern Iran, and the territory of the Persian Gulf. The hot air stretching over northeastern Africa and Saudi Arabia causing extreme pressure gradient over the studied region. This has paved the way for unstable weather [50].

The spatial-temporal distribution of the second precipitation pattern of fall for the AT in the Middle East (Figure 6B) shows a low wide system. This low system has moved the cold air of upper latitudes toward the lower ones. Since it crosses the Black Sea and the eastern Mediterranean, it has also transferred humidity to northern parts of the studied region. During the dominance of this pattern, air flows that have stretched over central and southern parts of the Middle East have not transferred cold air to the studied region because of their low latitude. This has caused extreme pressure gradient and instability in northern parts of the Middle East. At the same time, a hot air mass has moved from northern Africa toward central and southern regions in the Middle East. Thus, southern parts of the Middle East have maximum AT (5650 to 5750 m), while northern parts have minimum thickness.

There are two low cores in the Mediterranean and southwestern Europe (Figure 6C), which are the third precipitation pattern of fall for the AT. They have directed eastward flows toward northern Africa. On the other hand, a deep trough is located over northern parts of the Middle East. In the western part, the trough has caused the movement of cold air from northern Europe toward northern regions of the Middle East. It has led to blocking in central Turkey, and has caused cold air advection toward the Middle East on a wide scale.

On the other hand, central parts of the Middle East are influenced by the hot air of North Africa. Thus, an extreme pressure gradient has been formed over northern and central parts of the Middle East, which is clearly observed in the density of iso height contours. The movement of cold air of upper latitudes over northern regions of the Middle East has increased the density of AT, hence reducing AT. Thus, AT is 5700 m in southern Saudi Arabia because this region is completely influenced by the hot air of North Africa. Extreme difference in AT between southern and northern regions of the Middle East indicates that the extreme temperature difference dominates the AT of the region.

The last precipitation pattern of fall for the AT in the Middle East is presented in Figure 6D. It has prevented the entrance of cold and humid air of the Mediterranean toward northern parts of Africa. On the other hand, the zonal-based nature of air flows in North Africa and their movement toward southern parts of the Middle East show the advection of hot air in the studied region. In addition to this phenomenon, the movement of cold air from Europe through a deep European trough has caused the formation of a baroclinic atmosphere, a front, and finally instability in northern parts of the Middle East. The maximum degree of baroclinicity and instability can be observed in northern parts of Saudi Arabia, Iraq, and western parts of Iran. This has led to the movement of humidity from the Mediterranean, the Black Sea, and the Red Sea, and has caused pervasive precipitations in the studied region.

5. Conclusions

Variations in AT can influence atmospheric events. Atmospheric variations, which directly determine temperature conditions, play an important role in controlling climatic events. This study focused on analyzing AT in Iran and the Middle East. The results are summarized in the following lines:

Spatial distribution of average AT in Iran and the Middle East shows that, in winter, the average AT in Iran and the Middle East declines to the lowest degree because of the presence of pressure systems that have cold cores. In spring, however, the thickness rises given that subtropical high pressure systems gradually enter the region and cold systems withdraw to upper latitudes.

In summer, the Middle East is influenced by Azores subtropical high pressure. Thus, AT reaches its peak in this season. On the other hand, the highest degree of variations in AT is observed in fall, which is a transition period. This is attributed to the fact that, in this season, pressure systems of hot seasons are leaving the region, western pressure systems and winds are entering the area. The degree of variations is more clearly observed in upper latitudes. In all seasons, lower latitudes experience smaller coefficient of variations of AT (in comparison with upper latitudes). The smallest degree of variations in AT is observed in southern Saudi Arabia, the Arabian Sea, and the Persian Gulf. On the contrary, the highest degree of variations is recorded for northern parts of Iran, Turkey, and Syria.

Spatial-temporal variations of AT in the Middle East during winter show that a large area of the Middle East experiences a negative trend in AT during this season. The sharpest negative trend belongs to northern parts of Iran, Iraq, and Turkey. In contrast, the negative trend is weaker in spring and moves toward upper latitudes. Southern parts of the Middle East have a positive trend of AT reaching the highest degree in April. The same positive trend exists in summer too, with the maximum positive trend of AT (30 m) being recorded in July for southern parts of Saudi Arabia and the Red Sea. In fall, the positive trend of AT is weaker than that in summer. Thus, northwestern parts of Iran and Turkey experience a negative trend, while a positive trend still exists in the rest of the region.

Investigating and studying the atmospheric factors that cause Iran's precipitation, we observed that the occurrence of these precipitations is influenced by different air masses with different natures in the upper and lower latitudes. Thus, the most important atmospheric factors of precipitation control in Iran in SLP can be the East Mediterranean, Sudan, Saudi Arabia's low pressure systems, and the high pressures that are located on Europe and Kazakhstan. In upper-air, (500 Hpa) due to high Mediterranean trough and blocking phenomenon have made weather lasting for a long time. However, the predominant role in Iran's precipitations is played by the Mediterranean and Sudan's Low pressures. They create maximum pressure ingredient providing the basis for the creation of instability, which is an introduction to precipitation. However, the blocking systems have an important role in the deviation of the Western wind and creating ridge and troughs in the internal regions of Iran. That is accompanied by instability of the air, and the influx of cold air from the high-pressure systems of Europe. Which, in addition to the transporting European cold air, transmits moisture from the Mediterranean and Black Sea and have a major effect on Iran's precipitation. Occurrence of frosts was mainly influenced by five patterns, namely Siberian high-pressure and European high-pressure, deep trough pattern of Eastern Europe and Sudanese low pressure, dual-core pattern of Siberian high-pressure, deep Eastern European trough and polar low pressure pattern, and Omega pattern. The severest frosts occurred during the dominance of the Omega pattern [26]. Extreme and widespread precipitation in the northwest of Iran are caused by four patterns, which, in all of them, a trough is located in the west of Iran [50]. The coldest extreme low temperature of Iran occurred when negative anomaly of AT located over Siberian and northeastern parts of Iran and also positive anomaly observed over Barents Sea, Greenland and Europe [56].

References

1. Alijani, B. *Synoptic Climatology*, 1st ed.; SAMT Press: Tehran, Iran, 2006; Volume 1, p. 153. (In Persian)
2. Zhang, T.; Stamnes, K.; Bowling, S.A. Impact of the atmospheric thickness on the atmospheric downwelling longwave radiation and snowmelt under clear-sky conditions in the arctic and subarctic. *J. Clim.* **2001**, *14*, 920–939. [CrossRef]
3. Sutcliffe, R.C.; Forsdyke, A.G. The theory and use of upper air thickness patterns in forecasting. *Q. J. R. Meteorol. Soc.* **1950**, *76*, 189–217. [CrossRef]
4. Masoodian, S.A.; Karsaz, S. Synoptic analysis of thickness patterns at the time of heavy and extensive precipitations of south zagros area. *Geogr. Dev. Iran. J.* **2015**, *12*, 15–28. (In Persian)
5. Omidvar, K. *Synoptic Climatology*, 1st ed.; Yazd University Press: Yazd, Iran, 2010; Volume 1, p. 356. (In Persian)
6. Alijani, B.; O'Brien, J.; Yarnal, B. Spatial analysis of precipitation intensity and concentration in iran. *Theor. Appl. Climatol.* **2008**, *94*, 107–124. [CrossRef]
7. Ghaemi, H. *Generol Meteorology*; SAMT Press: Tehran, Iran, 2006; Volume 1, p. 591. (In Persian)
8. Mohammadi, B.; Masoudian, S.A. Synoptic analysis of heavy precipitation in iran case study november 1994. *Geogr. Dev.* **2010**, *19*, 47–70. (In Persian)

9. Sotodeh, F.; Alijani, B. The relationship between spatial distribution of heavy precipitation and pressure patterns in guilan province. *J. Spat. Anal. Environ. Hazards* **2015**, *2*, 63–73. (In Persian) [CrossRef]

10. Tabari, H.; Abghari, H.; Hosseinzadeh Talaee, P. Temporal trends and spatial characteristics of drought and rainfall in arid and semiarid regions of Iran. *Hydrol. Process.* **2012**, *26*, 3351–3361. [CrossRef]

11. Rousta, I.; Soltani, M.; Zhou, W.; Cheung, H.H. Analysis of extreme precipitation events over central plateau of iran. *Am. J. Clim. Chang.* **2016**, *5*, 297. [CrossRef]

12. Rousta, I.; Akhlagh, F.K.; Soltani, M.; Shabnam, S.M.T. Assessment of blocking effects on rainfall in northwestern iran. In Proceedings of the 12th International Conference on Meteorology, Climatology and Atmospheric COMECAP 2014, Athina, Grecce, 28–31 May 2014; Kanakidou, M., Mihalopoulos, N., Nastos, P., Eds.; Crete University Press: Athina, Grecce, 2014; p. 291.

13. Rousta, I.; Doostkamian, M.; Haghighi, E.; Ghafarian Malamiri, H.R.; Yarahmadi, P. Analysis of spatial autocorrelation patterns of heavy and super-heavy rainfall in iran. *Adv. Atmos. Sci.* **2017**, *34*, 1069–1081. [CrossRef]

14. Haghighi, E.; Jahanbakhsh, S.; Rezaee Banafshe, M.; Rousta, I. The study relationship between large-scale circulation patterns of sea level and snow phenomenon in the north west of iran. *Territory* **2016**, *12*, 19–35. (In Persian)

15. Rousta, I.; Nasserzadeh, M.; Jalali, M.; Haghighi, E.; Ólafsson, H.; Ashrafi, S.; Doostkamian, M.; Ghasemi, A. Decadal spatial-temporal variations in the spatial pattern of anomalies of extreme precipitation thresholds (case study: Northwest iran). *Atmosphere* **2017**, *8*, 135. [CrossRef]

16. Taimor, A.; Qhasem, A.; Rousta, I. Analyzing of 500 hpa atmospheric patterns in the incidence of prevassive and sectional rainfall in iran. *Plan. Arrange. Space Hum. Sci.* **2012**, *16*, 1–24. (In Persian)

17. Soltani, M.; Laux, P.; Kunstmann, H.; Stan, K.; Sohrabi, M.; Molanejad, M.; Sabziparvar, A.; SaadatAbadi, A.R.; Ranjbar, F.; Rousta, I. Assessment of climate variations in temperature and precipitation extreme events over iran. *Theor. Appl. Climatol.* **2016**, *126*, 775–795. [CrossRef]

18. Zhang, Y.; Sperber, K.; Boyle, J. Climatology and interannual variation of the east asian winter monsoon: Results from the 1979–95 ncep/ncar reanalysis. *Mon. Weather Rev.* **1997**, *125*, 2605–2619. [CrossRef]

19. Houssos, E.; Lolis, C.; Bartzokas, A. Atmospheric circulation patterns associated with extreme precipitation amounts in greece. *Adv. Geosci.* **2008**, *17*, 5–11. [CrossRef]

20. Azizi, G.; Akbari, T.; Davodi, M.; Akbari, M. Synoptic analysis of iran's 2008 sever cold. *Phys. Geogr. Res.* **2010**, *41*, 28–50. (In Persian)

21. Soltani, M.; Rousta, I.; Akhlagh, F.K.; Sh, S.M.T. Statistical synoptic analysis of summertime extreme precipitation events over kerman province, iran. In Proceedings of the 12th International Conference on Meteorology, Climatology and Atmospheric COMECAP 2014, Athina, Grecce, 28–31 May 2014; Kanakidou, M., Mihalopoulos, N., Nastos, P., Eds.; Crete University Press: Athina, Grecce, 2014; p. 291.

22. Asakereh, H. Frequency distribution change of extreme precipitation in zanjan city. *Geogr. Environ. Plan.* **2012**, *23*, 51–66. (In Persian)

23. Soltani, M.; Rousta, I.; Taheri, S.S.M. Using mann-kendall and time series techniques for statistical analysis of long-term precipitation in gorgan weather station. *World Appl. Sci. J.* **2013**, *28*, 902–908.

24. Sanders, F.; Davis, C.A. Patterns of thickness anomaly for explosive cyclogenesis over the west-central north atlantic ocean. *Mon. Weather Rev.* **1988**, *116*, 2725–2730. [CrossRef]

25. Struthwolf, M.E. Forecasting maximum temperatures through use of an adjusted 850- to 700-mb thickness technique. *Weather Forecast.* **1995**, *10*, 160–171. [CrossRef]

26. Rousta, I.; Doostkamian, M.; Haghighi, E.; Mirzakhani, B. Statistical-synoptic analysis of the atmosphere thickness pattern of iran's pervasive frosts. *Climate* **2016**, *4*, 41. [CrossRef]

27. Mohammadi, B. Evaluation of synoptic sea level pressure regions in warm half of the year. *Geogr. Thought* **2008**, *2*, 132–150. (In Persian)

28. Hossaini, S.M. Assessments of Synoptic Conditions in Caspian Sea Coasts. Master's Thesis, Esfahan University, Esfahan, Iran, 2009; p. 189. (In persian)

29. Soltani, M.; Zawar-Reza, P.; Khoshakhlagh, F.; Rousta, I. Mid-latitude cyclones climatology over caspian sea southern coasts–north of iran. In Proceedings of the 21st Conference on Applied Climatology, American Meteorological Society (AMS), American Meteorological Society, Westminster, CO, USA, 8–13 June 2014; Volume 1, pp. 1–3.

30. Halabian, A.; Hosseinali Pourjazi, F. Recognition the synoptic conditions of extreme and widespread precipitations in caspian western coasts by emphasis on atmosphere thickness patterns. *Sci. J. Manag. Syst.* **2012**, *2*, 101–122.

31. Nasrabadi, E.; Masoodian, S.A.; Asakereh, H. Comparison of gridded precipitation time series data in aphrodite and asfazari databases within iran's territory. *Atmos. Clim. Sci.* **2013**, *3*, 235. [CrossRef]

32. Masoodian, A.; Kiany, K.; Sadeqh, M. Introduction and a comparison among gridded precipitation database of asfazari with gpcc, gpcp and cmap. *Geogr. Res.* **2014**, *29*, 36–53. (In Persian)

33. Masoodian, S.; Darand, M. Synoptic analysis of extensive and persistent frosts in iran. *Geogr. Environ. Plan. J.* **2013**, *50*, 29–32. (In Persian)

34. Nazaripour, H. Calibration of rainfall-stream flow relationship for assessing and forecasting hydrological drought in kavir-e lut basin, Iran. *Sci. J. Manag. Syst.* **2017**, *9*, 73–90.

35. Asakereh, H.; Ashrafi, S.; Tarkarani, F. The relationship between precipitation status and daily temperature status in Iran. *Geogr. Dev.* **2014**, *12*, 81–93.

36. Balling, R.C.; Keikhosravi Kiany, M.S.; Sen Roy, S.; Khoshhal, J. Trends in extreme precipitation indices in Iran: 1951–2007. *Adv. Meteorol.* **2016**, *2016*. [CrossRef]

37. Ahmadi, M.; Dadashi, A. Assessment of the tracks of spatio-temporal precipitation, Iran. *Phys. Geogr. Res.* **2016**, *48*, 465–484. (In Persian)

38. Alijani, B. Spatial analysis of critical temperatures and daily precipitation in iran. *J. Geogr. Sci. Appl. Res.* **2011**, *20*, 9–30. (In Persian)

39. Ghavidel Rahimi, Y. *Synoptic Analysis with Grads Software*; SAHA Danesh Press: Tehran, Iran, 2016; Volume 2.

40. Lichtfouse, E.; Hamelin, M.; Navarrete, M.; Debaeke, P. *Sustainable Agriculture*; Springer: Berlin, Germany, 2009.

41. Priestley, M.B. *Spectral Analysis and Time Series*; Academic Press: London, UK, 1981; p. 353.

42. Vautard, R.; Yiou, P.; Ghil, M. Singular-spectrum analysis: A toolkit for short, noisy chaotic signals. *Phys. D Nonlinear Phenom.* **1992**, *58*, 95–126. [CrossRef]

43. Weedon, G.P. *Time-Series Analysis and Cyclostratigraphy: Examining Stratigraphic Records of Environmental Cycles*; Cambridge University Press: Cambridge, UK, 2003.

44. Pestiaux, P.; Van der Mersch, I.; Berger, A.; Duplessy, J.C. Paleoclimatic variability at frequencies ranging from 1 cycle per 10 000 years to 1 cycle per 1000 years: Evidence for nonlinear behaviour of the climate system. *Clim. Chang.* **1988**, *12*, 9–37. [CrossRef]

45. Yiou, P.; Genthon, C.; Ghil, M.; Jouzel, J.; Le Treut, H.; Barnola, J.; Lorius, C.; Korotkevitch, Y. High-frequency paleovariability in climate and co2 levels from vostok ice core records. *J. Geophys. Res. Solid Earth* **1991**, *96*, 20365–20378. [CrossRef]

46. Kendall, M.G.; Stuart, A. The advanced theory of statistics. In *Kendall1 the Advanced Theory of Statistics 1946*; Charles Griffin & Co.: London, UK, 1968.

47. Kaufman, L.; Rousseeuw, P.J. *Finding Groups in Data: An Introduction to Cluster Analysis*; John Wiley & Sons: Hoboken, NJ, USA, 2009; Volume 344.

48. Sarle, W.S. Finding groups in data: An introduction to cluster analysis. *J. Am. Stat. Assoc.* **1991**, *86*, 830–833. [CrossRef]

49. Zarrin, A.; Ghaemi, H.; Azadi, M.; Farajzadeh, M. The spatial pattern of summertime subtropical anticyclones over asia and africa: A climatological review. *Int. J. Climatol.* **2010**, *30*, 159–173. [CrossRef]

50. Rezaee Banafshe, M.; Hossein Alipour Ghazi, H.; Jaffari Shendi, F.; Alimohammadi, M. Synoptic analysis of heavy rainfall in northwest of iran (with an emphasis on patterns of atmospheric thickness). *Geogr. Plan.* **2015**, *19*, 117–135. (In Persian)

51. Amanollahi, J.; Kaboodvandpour, S.; Qhavami, S.; Mohammadi, B. Effect of the temperature variation between mediterranean sea and syrian deserts on the dust storm occurrence in the western half of iran. *Atmos. Res.* **2015**, *154*, 116–125. [CrossRef]

52. Shamsipour, A.; AlaviPanah, S.; Mohammadi, H.; Azizi, A.; Khoshakhlagh, F. An analysis of drought events for central plains of iran through an employment of noaa-avhrr data. *Desert* **2008**, *13*, 105–115.

53. Lashkari, H. Tracking sudanese low pressure systems to iran. *Hum. Sci. Res.* **2002**, *6*, 133–160. (In Persian)

54. Lashkari, H. *Synoptic Analysis of Heavy Precipitation in South Eastern Part of Iran*; Tarbiat Modarres University: Tehran, Iran, 1996.

55. Bagheri, J. The relationship between geopotential height 500 hPa circulation patterns with weather types of mountainous region of iran. *Geogr. Res.* **2010**, *25*, 153–176. (In Persian)

56. Darand, M.; Masoodian, A. Analysis of the anomalies of the severe cold patterns of iran in the period of 1960 to 2004. *Geogr. Res.* **2015**, *30*, 1–4.